Bulk electrical properties of rubrene single crystals: Measurements and analysis

D. Braga,* N. Battaglini, A. Yassar, and G. Horowitz†
ITODYS, Université Paris Diderot, CNRS-UMR 7086, 75205 Paris, Cedex 13, France

M. Campione, A. Sassella, and A. Borghesi
Dipartimento di Scienza dei Materiali, Università di Milano-Bicocca, Via Cozzi 53, 20125 Milano, Italy
(Received 30 July 2007; revised manuscript received 19 November 2007; published 17 March 2008)

Rubrene single crystals with well-developed (100) faces extending along the [010] direction were equipped with two planar gold electrodes deposited under low thermal load on the same crystal surface. The current-voltage curves measured on crystals with various thicknesses were analyzed by means of the space-charge-limited current model. In all cases, the curves present a clear trap-filled transition that allows extracting the trap-free mobility along the *b* axis. Working in a gap-type geometry and by comparing the mobility calculated from the Geurst two-dimensional and Mott–Gurney three-dimensional models, a clear 2D to 3D transition is established for a thickness that roughly corresponds to half the distance between the two electrodes. Further quantitative analysis of the data with a differential method leads to the conclusion that charge-transport properties at room temperature are affected by a discrete trap level pointing at 0.48 ± 0.02 eV above the valence band.

DOI: 10.1103/PhysRevB.77.115205 PACS number(s): 71.20.Rv, 72.80.Le, 72.20.Jv

I. INTRODUCTION

Rubrene, a tetraphenyl derivative of tetracene, has shown to form high quality single crystals that present high mobility[1,2] due to a very low density of defects and impurity related traps[2] and to cofacial π-stacking interaction in the *b* direction resulting in a very efficient electronic coupling.[3] This kind of organic solid is useful not only for device applications, but also for exploring the intrinsic properties of organic materials and investigating the upper limit of mobility in organic systems, since their characteristics are not affected by the imperfections of the film structure. The electrical properties of rubrene single crystals under field-effect conditions are now well documented.[4–7] However, even if the transistor structure provides a useful tool to analyze the charge transport in the regime of high charge density,[8] it cannot be used to determine the bulk parameters of the crystals, for which other techniques have to be employed. One of these is the analysis of the current-voltage (*I-V*) curves by means of the space-charge-limited current (SCLC) model,[9,10] an easy-to-handle method that, when properly managed, allows the determination of several charge-transport parameters, including mobility, density of free carriers, and concentration and energy distribution of traps. However, a strict way of conduct must be followed in order to avoid misinterpretation of the data.

In this work we present an electrical characterization of rubrene single crystals grown by physical vapor transport in a flowing stream of argon. Low thermal load deposition of gold on one surface of the crystals provided good Ohmic contacts with negligible nonlinear contribution. A set of electrical bulk parameters for the preferential growth direction is extracted from the experimental curves with a SCLC analysis. Particular attention is dedicated to the trap-free regime of these curves, from which it is possible to estimate the free-electron drift mobility and the density of the traps. We also show that the response of the crystals can be interpreted in terms of a discrete trap level at 0.48 eV above valence band edge, in good agreement with that recently found by means of temperature-dependent space-charge-limited current spectroscopy.[11]

II. EXPERIMENTAL TECHNIQUES

The rubrene crystals were grown by physical vapor transport[12] under a stream of argon and using proper cleaning process for all the glasses to avoid contamination with organic substances. This technique offers high quality crystals with large flat surfaces that are suitable for field-effect transistor fabrication. The crystal structure has been reported in the literature.[13,14] Rubrene crystals employed for the present study have tabular morphology with a well-developed (100) face with well-defined width, and elongated parallel to the [010] direction [see Fig. 1(a)]. Under the growth conditions described above, rubrene crystallizes in an orthorhombic phase with unit cell parameters $a=26.86$ Å, $b=7.19$ Å, and $c=14.43$ Å, containing four molecules arranged in a herringbone motif in the (100) plane and forming layers along the *a*-axis direction with spacing $a/2=13.43$ Å.[13] Because these crystals present higher mobility in the direction along the (100) face, we have used a gap-type geometry with two planar gold electrodes (approximate thickness of 30 nm) made by vacuum evaporation from an electrically heated tungsten wire. The gap was defined by a 25 μm diameter gold wire shadowing the semiconductor surface. To reduce the thermal load on the crystal surface during the deposition process, we used a thin tungsten wire ($\oslash=0.5$ mm) and small metal plates to mask the infrared radiation emanating from the warmest part of the wire. All the measurements were performed in the *bc* plane of the crystals, in dark and under argon atmosphere with a Keithley 4200 semiconductor parameter analyzer, using a linear stepwise increase of the

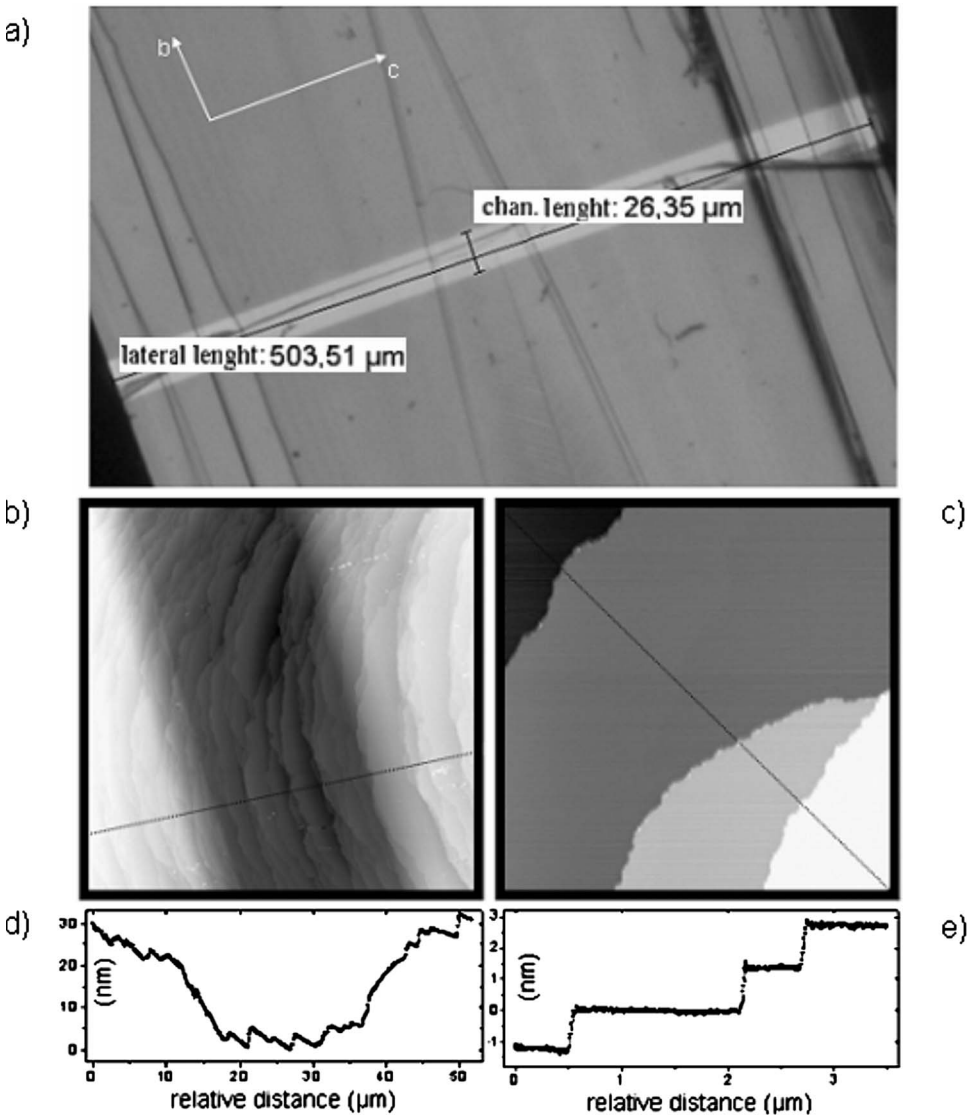

FIG. 1. (a) Optical microscope (a) and AFM [(b) and (c)] images of a rubrene crystal equipped with two gold planar contacts defined by means of a 25 μm shadow mask. (b) is a general and (c) a close view of the channel (d) and (e) are the respective profiles.

applied voltage and measuring the quasiequilibrium current (the transit time of the electron is less than the period of the applied electrical signal). The maximum applied voltage was 210 V corresponding to an electric field of 8.4×10^4 V/cm. After each measurement the sample was left in argon atmosphere for a few minutes to avoid heating by Joule effect. The surface morphology of the crystals and the parameters of the channels (shape and real length) were investigated using a Digital Nanoscope III*a* atomic force microscope (AFM) in tapping mode, whereas the crystal dimensions were determined with the aid of an optical microscope Olympus SZX12 coupled to an imaging software (except for the submicron samples, the thickness of which were determined with the AFM). Figure 1 shows the optical and morphological analyses of a representative crystal. The AFM analysis [Figs. 1(c)–1(e)] shows the shape of the channel and the morphology of the crystal surface [the thickness of the steps in Fig. 1(d) corresponds to the value $a/2$], while the optical microscope image [Fig. 1(a)] points out the homogeneity of the channel and its lateral dimension W.

III. RESULTS AND DISCUSSION

A. Charge injection

Prior to SCLC analysis, we checked the quality of the gold contacts. Good contacts should behave as infinite reservoirs of charge, so that only a negligible fraction of the applied voltage is absorbed across the interface. When this condition is fulfilled, the total current across the crystal is dominated by the bulk properties of the sample.[15] Two representative examples are illustrated in Figs. 2 and 3 for a good and a bad contact, respectively. Since the area and the quality of both contacts will unavoidably present some differences, the unsymmetrical character of the *I-V* curve in Fig. 3 can be interpreted as the sign that the current is limited by the contacts. Conversely, the perfectly symmetrical curve in Fig. 2 tells us that the current in this case is limited by the bulk of the crystal; that is, the current is bulk limited rather than contact limited. The linear (Ohmic) regime at very low bias (inset in Fig. 2) also indicates that the nonlinear Schottky barrier formed at the metal-semiconductor interface is in this case negligible. This behavior shows that a low

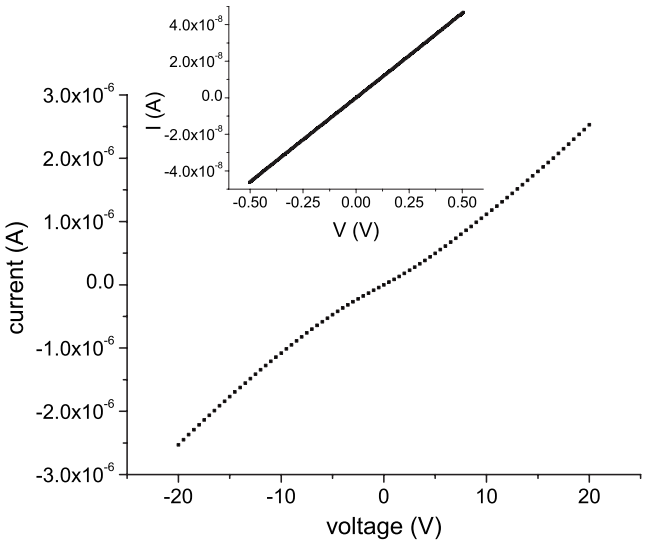

FIG. 2. Current vs applied voltage for an Ohmic rubrene-gold system. The inset shows the lack of non-Ohmic effect of a low voltage.

thermal load evaporation of gold on the surface of the crystals can provide good contacts. In all the remainder of the work, such crystals, for which unsymmetrical curves were recorded, were systematically disregarded.

B. Space-charge-limited current in a gap-type structure

Two basic architectures can be used for a SCLC analysis: the sandwich-type geometry [three dimensional (3D)], in which the electrodes are on the opposite face of the semiconductor, and the gap structure [two dimensional (2D)] where both electrodes are deposited on the same side of the film (or crystal). As pointed out by Grinberg *et al.*,[16] two limiting cases can be considered in the gap structure. In the first one, the thickness h of the semiconductor is very small ($h \to 0$),

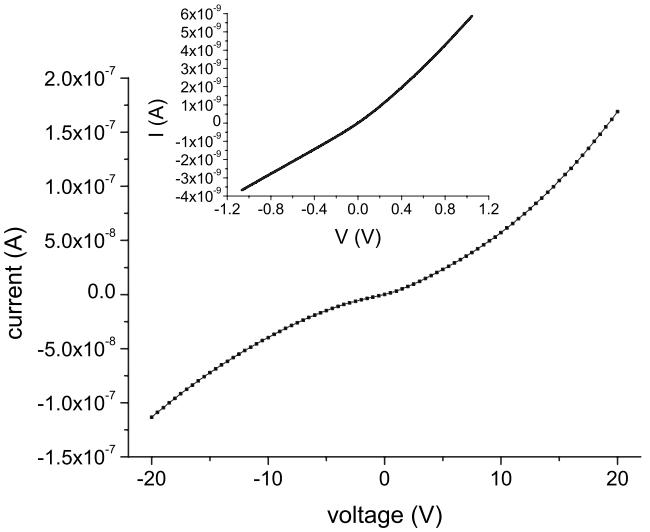

FIG. 3. Current vs applied voltage for an asymmetrical rubrene-gold contact with the inset showing problem linked to the different behavior of the contacts.

which corresponds to the 2D geometry first analyzed by Geurst[17] and Zuleeg and Knoll.[18] The second case intervenes when the thickness h is higher than the distance between electrodes L; under such circumstances, the current is h dependent and can be described by an equation similar to that originally developed by Mott and Gurney for the 3D (sandwich) architecture.[19] In each of these limiting cases, the current I is given by Eqs. (1) and (2), respectively.

$$I\frac{L^2}{W} = \frac{2}{\pi}\varepsilon\mu V^2 \quad \text{(film)}, \tag{1}$$

$$I\frac{L^2}{W} = \frac{9}{8}\varepsilon\mu\frac{h}{L}V^2 \quad \text{(bulk)}, \tag{2}$$

where L is the distance between the two electrodes, W the width of the channel, and h the thickness of the sample. μ is the mobility, ε the permittivity, and V the applied voltage. The general feature of the current flow in a thin film is, therefore, an Ohmic behavior at low applied voltage followed by a transition to a new regime in which $I \propto V^2/L^2$, in contrast to the $1/L^3$ dependence expected from the 3D analysis. Following Geurst,[17] it is possible to explain this behavior by looking at the electric field perpendicular to the semiconducting layer and therefore perpendicular to that one driving the charges over the distance L.

On account of the previous considerations, it is plausible to assume that a single crystal of thickness $h \gg 0$ with both electrodes on the same face is in an intermediate situation between the 2D and 3D cases, depending on the ratio between the two parameters h and L; when varying the ratio h/L, the coefficient in the Mott–Gurney's equation actually assumes a different weight with respect to $2/\pi$. Accordingly, it can be expected that the 2D law will dominate as long as $h/L \ll 1$, while the 3D law will be valid when $h/L \gg 1$, or more precisely as long as $(9/8)(h/L) \gg (2/\pi)$.

A common practice to discriminate between the two limiting cases consists of plotting the current at a given voltage as a function of the electrode distance, which is expected to vary as L^{-2} in a film structure ($h \ll L$) and as L^{-3} in a bulk structure ($h \gg L$).[13] Unfortunately, such an analysis could not be performed with our data. The reason is that the transition point between the Ohmic and SCLC regimes increases as L^2 (see below). With the technique used in this work, where the length of the channel is defined by a mask made of a calibrated gold wire, practical values of L were 25 μm, 50 μm, and above. The transition can therefore be expected to be four times larger with 50 μm than with 25 μm, with the consequence that the SCLC regime starts outside the explored voltage (0–200 V); so we had to restrict our analysis to devices with $L=25$ μm.

To bring evidence for a transition between the film and bulk regimes we have analyzed the dependence of the free-electron mobility μ (the mobility extracted from the I-V curves in the trap-free regime, that is, after the sharp current increase due to trap filling) on the crystal thickness using both Eqs. (1) and (2). Figure 4 illustrates the variation of the calculated mobility for crystals with various thicknesses and identical channel lengths ($L=25$ μm). It can be seen that, for

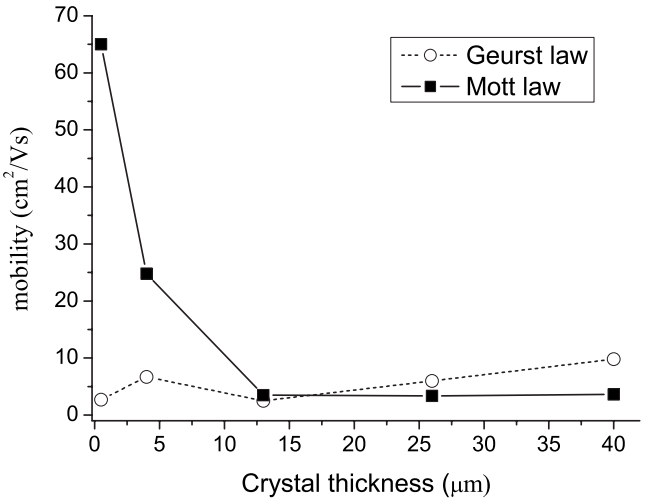

FIG. 4. Calculated mobility vs crystal thickness as derived from Eqs. (1) and (2). The channel length is constant and equal to 25 μm. The mobility value extracted with the Mott–Gurney law for the thick samples is approximately equal to 3.5 cm^2/V s.

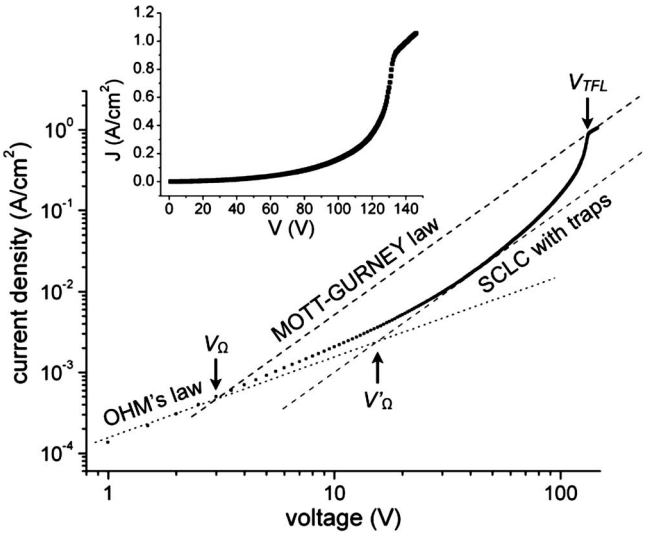

FIG. 5. Current density vs applied voltage in double-logarithmic and linear (inset in the figure) scales for an ~13 μm thick rubrene single crystal at room temperature. Four different regimes are clearly observable: (i) at low voltage the current rises linearly and (ii) becomes SCL at higher field. Up till the (iii) transition point V_{TFL} the properties are still determined by traps, to the point they become filled and a regime given by the Mott–Gurney law (iv) [see Eq. (2)] takes place.

thicknesses comparable to or greater than the channel length (15 $\mu m < h < 40$ μm), the Mott–Gurney law gives a thickness independent mobility of around 3.5 cm^2/V s. At lower thicknesses, a sharp rise of the calculated mobility occurs. This is because, when the cathode-anode spacing becomes larger than the crystal thickness, Eq. (2) loses its physical meaning and, although it is an approximate description of the system, the Geurst law has to be used (a more reliable theory would have to consider the finite thickness of the crystal). A converse behavior is followed by the 2D mobility; that is, at low thicknesses, the 2D mobility magnitude is comparable to that of the 3D mobility at high thickness, while it tends to depart from this mean value as the thickness increases. In conclusion, Fig. 4 brings evidence for a transition between a 2D and a 3D regime. The fact that the transition point occurs at $h \simeq 13$ μm, that is, when $(9/8)(h/L) \simeq (2/\pi)$ brings additional evidence for such a transition.

We note that above the transition point, the 3D mobility is independent of the thickness of the crystal, which can be interpreted by stating that the current density is uniform over the whole section of the crystals. At this point, the question arises as to how can the charge carriers be uniformly injected in the whole thickness while the contacts are only located on one side? 3D modeling would be required to give a definitive answer to that, but we can put forward a simple image where the mobility in the direction across the crystal of the charges is high enough to provide a uniform repartition of the injected charge. Of course, such a process would not operate for very thick crystals; however, this limitation is not reached in the present case.

C. Bulk parameter extraction

Within the thickness domain where the Mott–Gurney model provides a good description of the system, a set of electrical parameters is easily extracted from the experimental curves. We show in Fig. 5 a representative experimental *I-V* curve in linear and double-logarithmic scales.

At low voltages, the curve follows an Ohmic (linear) regime, due to the presence of thermal free carriers related to shallow defect states, that at room temperature does not act like effective charge traps. Upon increasing the applied voltage, a transition from this regime to a square law regime occurs. From the Mott–Gurney theory we know that such a trend can be described by

$$J = \frac{9}{8}\theta\epsilon\mu\frac{V^2}{L^3}, \tag{3}$$

where the trap parameter $\theta = n/(n+n_t)$ is the ratio between the density of free carriers achieved under injection, n, and the total density of injected carriers, trapped n_t, and free. Therefore this regime is linked to the presence of a discrete trap level that reduces the measured (or effective) charge carrier mobility $\mu_{eff} = \theta\mu$ and affects the space-charge-limited current. Note that if $n_t \gg n$, the trap parameter reduces to $\theta \simeq n/n_t$. Given the voltage $V_{\Omega'}$ at which the transition between the Ohmic and SCLC regimes with traps occurs, an estimation of the thermally generated electron density n_0 is possible by using the equation $n_0 = V_{\Omega'}\theta\varepsilon V/eL^2$. At higher voltages, the current experiences an almost vertical rise (as predicted by the Lambert regional approximation method) and reaches the so-called trap-free regime at an applied voltage $V_{TFL} = eN_tL^2/\varepsilon$, where N_t is the density of traps and e the elemental charge. Actually, at V_{TFL} the amount of charge injected by the contact is sufficient to fill the traps, so that the quasi-Fermi level establishes at a level above the trap distribution within the energy gap; accordingly, the mobility is no more affected by impurity or

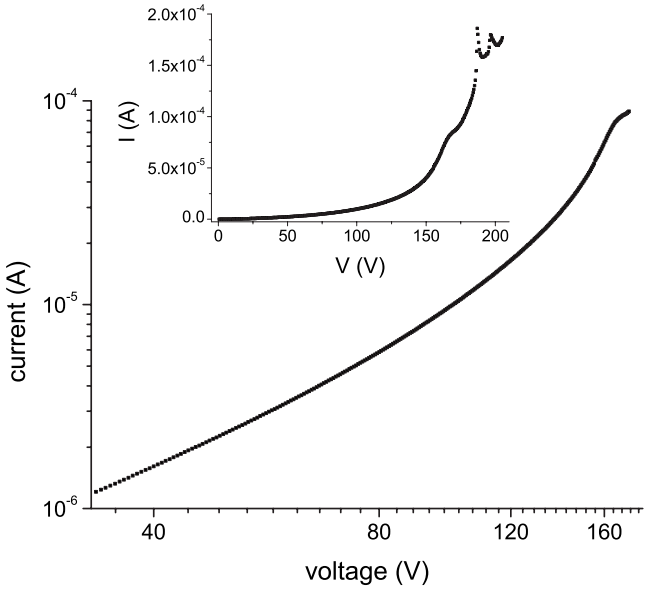

FIG. 6. *I-V* characteristic of a 560 nm thick rubrene crystal with gold electrodes on the surface and a channel length of 25 μm in double-logarithmic scale and linear scale (inset in the figure). The inset shows the complete experimental characteristic, whereas, for clarity, in the logarithmic plot only the SCLC behavior is reported.

defects states. Under such circumstances, all additional carriers introduced are essentially free, so the free-electron mobility μ can be estimated from Eq. (3) with $\theta=1$. Access to the trap-free mobility is obtained in the rare case when the density of trap is significantly low (otherwise the semiconductor is damaged before that limit is attained). We note also that the knowledge of V_{TFL} makes it possible to estimate the density of traps N_t from the experimental *I-V* curves. However, it should be pointed out that this is only valid under the assumption that the traps are uniformly distributed in the volume of the crystal, which is most often an oversimplification, because the density of traps at the interface is always different from that in the bulk.[8]

When analyzing the experimentally determined triangle of Lampert and Mark[9] reported in Fig. 5, we also see that the presence of shallow trapping delays the finish of the Ohmic regime from the critical voltage V_Ω to $V_{\Omega'}=(1/\theta)V_\Omega$ in agreement with the discrete trap level theory (the ratio between V_Ω and $V_{\Omega'}$ is equivalent to θ).

All the curves used to estimate the reliance of the mobility on the crystal thickness (Fig. 4) present the same trend: a square-law dependence at low voltage followed by a sharp current increase and a second square-law region at higher current. The *I-V* curve for a 560 nm thick rubrene crystal is reported as a further example in logarithmic and linear scales (Fig. 6). The trap-free region is preceded by a square-law section and by an increase of the current due to trap filling. We also observe a second vertical rise, a characteristic found also in some thick crystals, that could represent either the filling of another discrete trap level, or the breakdown of the system at high injected current density.

The electrical parameters for two thick crystals are given in Table I. All the numbers are extracted by analyzing the experimental *I-V* curves with Mott–Gurney's equation [Eq. (3)]. The trap constant θ is calculated from the ratio between the effective μ_{eff} and trap-free μ mobility, but the same value can be found by considering that in the $\log J-\log V$ plot the trap limited curve is shifted below the trap-free curve by θ. The density of thermal carriers n_0 is estimated knowing θ and the transition potential $V_{\Omega'}$. The in-plane rubrene static dielectric constant was assumed to be $\varepsilon_r=2.6$, the mean value extrapolated from the crystal full dielectric tensor at $\omega=0$.[20]

TABLE I. Set of electrical parameters for two different rubrene crystals, calculated with the Mott–Gurney theory with a discrete trap level.

	Sample I[a]	Sample II[b]
μ (cm^2/V s)	3.5	3.4
μ_{eff} (cm^{2}2/V s)	0.74	0.72
n_0 (cm^{-3})	5.7×10^{11}	8.8×10^{11}
N_t (cm^{-3})	5.2×10^{13}	4.2×10^{13}
θ	0.2	0.2

[a]Crystal thickness $h=13$ μm.
[b]Crystal thickness $h=26$ μm.

D. Space-charge-limited current differential method: The discrete trap level energy

To avoid incorrect interpretation of the SCL trend in the *I-V* curves, but also because in many samples the complete trap-free regime is followed by an electrical breakdown (Fig. 7), we have also analyzed the characteristics in terms of the SCLC differential method.[21] This technique, a general starting point for determining bulk localized states,[22] is based on the assumption that on changing the position of the quasi-Fermi level E_F (by increasing the voltage applied to the sample), one can determine the distribution of traps for which the occupancy is changed. Moreover it represents a straightforward tool to prove the consistency of the experi-

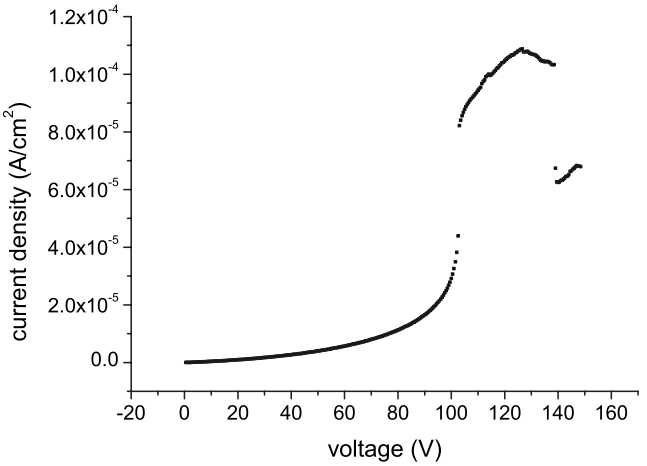

FIG. 7. Current vs applied potential in a rubrene single crystal. The trap-free regime is followed by a breakdown of the system. This event could lead up to misunderstanding and bad interpretation of the vertical rise that precedes it.

mental results with the simple Mott–Gurney discrete trap SCLC model and to exclude any misinterpretation of the data, such as assigning the square-law dependence to a discrete trap level instead of a monotonously increasing slope,[10] followed by double injection effects.[9,23,24]

In the framework of the SCLC analysis, using the zero-temperature statistic, it is possible to estimate the parameters of an arbitrary distribution of traps, knowing the function describing the distribution $h(E_F)$

$$h(E_F) = \frac{\kappa_1 \kappa_2 \epsilon V}{2eL^2 kT(m-1)} \tag{4}$$

and the position of the quasi-Fermi level at the noninjecting electrode $E_F(L)$ as follows:

$$E_F(L) = kT \ln \frac{L}{\kappa_1 N_v e \mu} + kT \ln \frac{J}{V}. \tag{5}$$

Here, $m = \mathrm{d} \ln J / \mathrm{d} \ln V$, L is the distance between the electrodes, N_v the effective density of states in the highest occupied molecular orbital, and the parameters κ_1 and κ_2 are the average distance of the injected charge from the anode and the ratio of the carrier concentration at the anode to the injection carrier concentration, respectively. These parameters are related to the slope of the characteristic by the equations[25]

$$\kappa_1 = \frac{2m-1}{m}, \tag{6}$$

$$\kappa_2 = \frac{m-1}{m}(1+B), \tag{7}$$

where B is a second-order correction that can be neglected to a first approximation.

Equations (4) and (5) allow us to extract, in principle, an energy distribution of states directly from a single experimental *I-V* curve. However, an obvious problem is that, according to Eq. (5), the effective density of states N_v should be previously known in order to find the correct values of the trap energy depth. This need, combined with the approximation of uniformity in the trap distribution, makes the calculated trap depth E_t only an estimation of the real value, altered by an error that may be as great as several kT. However, the found distribution, if correctly fitted, can be used to properly assign the SCL behavior and hence confirm the reliability of the parameters obtained with the Mott–Gurney analysis.

With this in mind, taking $N_v = 1 \times 10^{21}$ cm^{-3},[26] we have used Eqs. (4) and (5) to estimate the density of those traps whose occupancy changes during the voltage sweep. For that, we have performed a fitting of the data with the bell-shaped distribution derived by Nešpurek to explain the effect of the temperature on the visibility of discrete trap levels as follows:

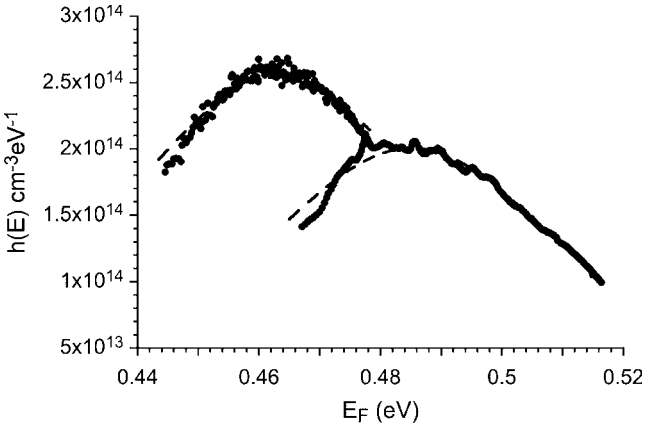

FIG. 8. Density of states [Eqs. (4) and (5)] and fitting curve to Eq. (8) for two different crystals. The band edge is chosen as the reference level. Using the room temperature value $kT = 25 \times 10^{-3}$ eV, the following fitting trap parameters are obtained: $N_t = 4 \times 10^{14}$ cm^{-3} and $E_t = 0.485$ eV (data on the left hand side), $N_t = 5.1 \times 10^{14}$ cm^{-3} and $E_t = 0.462$ eV (data on the right hand side). We have removed from the DOS reconstruction the apparent distribution maxima appearing in the low-energy region when it falls down the necessary condition $\theta \ll 1$.

$$n_t(E_F) = N_t \frac{\exp\left(\frac{E_t - E_F}{kT}\right)}{\left[1 + \exp\left(\frac{E_t - E_F}{kT}\right)\right]^2}, \tag{8}$$

where $n_t(E_F)$ is the density of trapped carriers, N_t and E_t are the density and the energy depth of the discrete trap, and E_F the quasi-Fermi level given by Eq. (5). N_t and E_t are in this case the fitting parameters. Actually, fitting the data with this equation is possible because the experimentally accessible parameter is not the energetic distribution $h(E)$, but the density of trapped carriers $n_t(E)$ [strictly speaking, Eq. (4) is only valid at low temperature, under the zero-temperature approximation where $h(E) \simeq n_t(E)$]. Figure 8 shows the energetic distributions (scattered data) and the fitting curves (dashed lines) for two different samples. It can be seen that the distributions are satisfactorily fitted to Eq. (8) at room temperature ($T = 300$ K). This confirms that within the voltage explored, the SCL features are essentially related to a discrete trap level located at $E_t = 0.48 \pm 0.02$ eV above the valence band and with a density $N_t = (4 \pm 2) \times 10^{14}$ cm^{-3} (the uncertainty is estimated from the spreading of the fitting parameters from one crystal to the other). A comparable discrete trap state level at about the same energy was found in the density of states (DOS) of rubrene recently reported by Krellner *et al.*[11]

It is worth remembering that the thus derived trap distribution is only valid in the region of the forbidden energy gap

lying between E_{F0} and E_{Fh}, that is, between the position of the Fermi level at equilibrium and the position of the quasi-Fermi level at the highest voltage applied to the crystal during the experimental run. Our measurements were made at room temperature and the corresponding energy range does not extend outside this discrete level, even if we cannot exclude that a continuum of localized trapping states is also present in this region of the energy gap (and in the energy region closer to the valence band edge). In any case these states make a negligible contribution to the SCLC characteristic because they act like a background in the presence of the dominant discrete trap. Therefore the free-carrier mobility found through the SCLC analysis is characteristic of charge carriers not affected by a discrete trap level, but it may be guessed that, if higher-energy states could be reached, that is, higher voltages could be applied, even greater mobility values would be found.

IV. CONCLUSIONS

We have analyzed the in-plane hole transport properties of rubrene single crystals by means of the space-charge-limited current model and established a set of electrical parameters that characterize the carrier motion. The *I-V* curves show a trap-free SCLC regime that allows us to determine a trap-free mobility of the charge carriers of 3.5 cm^2/V s. Working in a gap-type structure and by calculating the mobility within the Geurst 2D and Mott–Gurney 3D models for various crystal thicknesses, we found a transition between the 2D and 3D regimes at a thickness corresponding to roughly half the distance between the electrodes. From a differential analysis of the *I-V* curves, we have also found that the room temperature electrical features are related to a discrete trap level at 0.48 ± 0.02 eV above the valence band.

*Also at Università di Milano-Bicocca, Dipartimento di Scienza dei Materiali, Milano, Italy; daniele.braga@mater.unimib.it
†horowitz@univ-paris-diderot.fr

[1] V. Podzorov, E. Menard, A. Borissov, V. Kiryukhin, J. A. Rogers, and M. E. Gershenson, Phys. Rev. Lett. **93**, 086602 (2004).
[2] R. Zeis, C. Besnard, T. Siegrist, C. Schlockermann, X. L. Chi, and C. Kloc, Chem. Mater. **18**, 244 (2006).
[3] D. A. da Silva Filho, E.-G. Kim, and J.-L. Bredas, Adv. Mater. (Weinheim, Ger.) **17**, 1072 (2005).
[4] A. L. Briseno, S. C. B. Mannsfeld, M. M. Ling, S. H. Liu, R. J. Tseng, C. Reese, M. E. Roberts, Y. Yang, F. Wudl, and Z. N. Bao, Nature (London) **444**, 913 (2006).
[5] C. Goldmann, C. Krellner, K. P. Pernstich, S. Haas, D. J. Gundlach, and B. Batlogg, J. Appl. Phys. **99**, 034507 (2006).
[6] A. L. Briseno, R. J. Tseng, M. M. Ling, E. H. L. Talcao, Y. Yang, F. Wudl, and Z. N. Bao, Adv. Mater. (Weinheim, Ger.) **18**, 2320 (2006).
[7] T. Takenobu, T. Takahashi, J. Takeya, and Y. Iwasa, Appl. Phys. Lett. **90**, 013507 (2007).
[8] R. W. I. de Boer, M. E. Gershenson, A. F. Morpurgo, and V. Podzorov, Phys. Status Solidi A **201**, 1302 (2004).
[9] M. A. Lampert and P. Mark, *Current Injection in Solids* (Academic, New York, 1970).
[10] E. A. Silinsh, *Organic Molecular Crystals: Their Electronic States* (Springer-Verlag, Berlin, 1980).
[11] C. Krellner, S. Haas, C. Goldmann, K. P. Pernstich, D. J. Gundlach, and B. Batlogg, Phys. Rev. B **75**, 245115 (2007).
[12] R. A. Laudise, C. Kloc, P. G. Simpkins, and T. Siegrist, J. Cryst. Growth **187**, 449 (1998).
[13] O. D. Jurchescu, A. Meetsma, and T. T. M. Palstra, Acta Crystallogr., Sect. B: Struct. Sci. **62**, 330 (2006).
[14] B. D. Chapman, A. Checco, R. Pindak, T. Slegrist, and C. Kloc, J. Cryst. Growth **290**, 479 (2006).
[15] A. Moliton, *Optoelectronics of Molecules and Polymers* (Springer, New York, 2005).
[16] A. A. Grinberg, S. Luryi, M. R. Pinto, and N. L. Schryer, IEEE Trans. Electron Devices **36**, 1162 (1989).
[17] J. A. Geurst, Phys. Status Solidi **15**, 107 (1966).
[18] R. Zuleeg and P. Knoll, Appl. Phys. Lett. **11**, 183 (1967).
[19] N. F. Mott and R. W. Gurney, *Electronic Processes in Ionic Crystals* (Clarendon, Oxford, 1940).
[20] S. Tavazzi, A. Borghesi, A. Papagni, P. Spearman, L. Silvestri, A. Yassar, A. Camposeo, M. Polo, and D. Pisignano, Phys. Rev. B **75**, 245416 (2007).
[21] S. Nešpurek and J. Sworakowski, J. Appl. Phys. **51**, 2098 (1980).
[22] O. Zmeškal, F. Schauer, and S. Nešpurek, J. Phys. C **18**, 1873 (1985).
[23] H. T. Henderson, K. L. Ashley, and M. K. L. Shen, Phys. Rev. B **6**, 4079 (1972).
[24] R. H. Bube, J. Appl. Phys. **33**, 1733 (1962).
[25] J. Sworakowski and S. Nešpurek, IEEE Trans. Electr. Insul. **24**, 223 (1989).
[26] R. W. I. de Boer and A. F. Morpurgo, Phys. Rev. B **72**, 073207 (2005).